Thermoelectric phase diagram in a $CaTiO_3$–$SrTiO_3$–$BaTiO_3$ system

Masahiro Yamamoto
Graduate School of Engineering, Nagoya University, Furo-cho, Chikusa, Nagoya 464-8603, Japan

Hiromichi Ohta and Kunihito Koumoto[a)]
Graduate School of Engineering, Nagoya University, Furo-cho, Chikusa, Nagoya 464-8603, Japan and CREST, Japan Science and Technology Agency, 4-1-8 Honcho, Kawaguchi 332-0012, Japan

(Received 12 December 2006; accepted 15 January 2007; published online 12 February 2007)

Herein the authors propose a compositional thermoelectric phase diagram, which includes the density of states effective mass (m_d^*) carrier relaxation time (τ), and thermoelectric power factor ($S^2\sigma$, where S and σ are Seebeck coefficient and electrical conductivity) for high-quality epitaxial films composed of 20%-Nb-doped $CaTiO_3$–$SrTiO_3$–$BaTiO_3$ solid solutions [$(Ca,Sr,Ba)\times(Ti_{0.8}Nb_{0.2})O_3$]. The m_d^* values almost proportionally increase with the in-plane lattice parameter of $(Ca,Sr,Ba)(Ti_{0.8}Nb_{0.2})O_3$ epitaxial film, while the τ values drastically decrease when Ca and/or Ba are substituted for Sr in $Sr(Ti_{0.8}Nb_{0.2})O_3$, indicating that the Sr-site substitution negatively affects the thermoelectric performance of Nb-doped $SrTiO_3$. © *2007 American Institute of Physics*. [DOI: 10.1063/1.2475878]

Recently, complex metal oxides such as heavily electron-doped $SrTiO_3$,[1–3] Na_xCoO_2 ($x\sim0.7$),[4,5] and $Ca_3Co_4O_9$ (Refs. 6–8) have attracted much attention for generating thermoelectric power at high temperatures ($\sim$1000 K). Although 20%-Nb-doped $SrTiO_3$ [$Sr(Ti_{0.8}Nb_{0.2})O_3$] (Refs. 9–11) exhibits the largest thermoelectric figure of merit ($ZT=S^2\sigma T\kappa^{-1}$, S: Seebeck coefficient, σ: electrical conductivity, T: absolute temperature, and κ: thermal conductivity) among reported n-type metal oxides of $\sim$0.37 at 1000 K, the performance is insufficient to generate thermoelectric power at high temperatures using waste heat from automobiles and industrial plants.

Muta *et al.*[12,13] have reported that Sr-site substitution of $SrTiO_3$ with Ca or Ba may be a good way to improve ZT of Nb-doped $SrTiO_3$ because these substitutions may efficiently reduce the lattice thermal conductivity due to the fact that alloying scatter phonons if the substitution does not affect the electron transport properties. In order to clarify whether substituting the Sr site in $Sr(Ti_{0.8}Nb_{0.2})O_3$ affects the electron transport properties, we measured the carrier transport and thermoelectric properties of high-quality epitaxial films of 20%-Nb-doped $CaTiO_3$–$SrTiO_3$–$BaTiO_3$ solid solutions [hereafter referred to as $(Ca,Sr,Ba)(Ti_{0.8}Nb_{0.2})O_3$] at room temperature (300 K). Consequently, we established a thermoelectric phase diagram for the $(Ca,Sr,Ba)(Ti_{0.8}Nb_{0.2})O_3$ system. Although the density of states effective mass (m_d^*) increases almost proportionally with the in-plane lattice parameter of $(Ca,Sr,Ba)(Ti_{0.8}Nb_{0.2})O_3$ film, the carrier relaxation time (τ) drastically decreases when Ca and/or Ba are substituted for Sr in $Sr(Ti_{0.8}Nb_{0.2})O_3$, indicating that Sr-site substitution negatively affects the thermoelectric performance of $Sr(Ti_{0.8}Nb_{0.2})O_3$.

Epitaxial films of $(Ca,Sr,Ba)(Ti_{0.8}Nb_{0.2})O_3$ were grown on the (001) face of a stepped $LaAlO_3$ substrate[14] at 900 °C by pulsed laser deposition (Pascal) using a KrF excimer laser (Lambda Physik COMPex 102, 20 ns, $\sim$1 J cm^{-2} pulse^{-1}, 10 Hz) as an ablation light source. Details of our film growth technique have been reported elsewhere.[9,11] Film thickness, crystallographic orientation, and lattice parameters of the resultant films were evaluated by high-resolution x-ray diffraction (HRXRD, Cu $K\alpha_1$, ATX-G, Rigaku Co.). The surface morphologies of the films were analyzed by an atomic force microscope (AFM) (Nanoscope E, Digital Instruments).

The resultant films were $\sim$40 nm thick, which were precisely measured by the out-of-plane HRXRD and grazing incidence x-ray reflectivity. Intense streak patterns are observed in the reflection high energy electron diffraction (RHEED) pattern of the films [Fig. 1(a) inset], indicating that the $(Ca,Sr,Ba)(Ti_{0.8}Nb_{0.2})O_3$ films are heteroepitaxially grown on the (001) face of $LaAlO_3$, while an epitaxial relationship of $(001)[100](Ca,Sr,Ba)(Ti_{0.8}Nb_{0.2})O_3\|(001)\times[100]LaAlO_3$ is maintained. Atomically flat terraces and

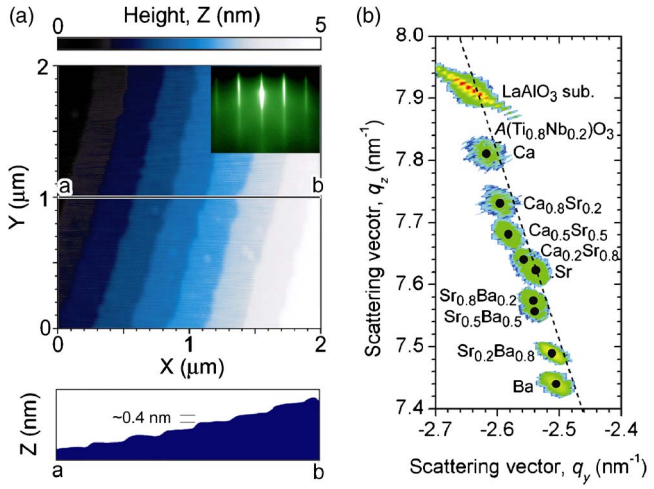

FIG. 1. (Color online) Crystallographic evaluation of $(Ca,Sr,Ba)\times(Ti_{0.8}Nb_{0.2})O_3$ films. (a) Topographic AFM image of a $(Ca_{0.4}Sr_{0.2}Ba_{0.4})\times(Ti_{0.8}Nb_{0.2})O_3$ film with clear atomically flat terraces and steps ($\sim$0.4 nm). Typical RHEED pattern of the film with an intense streak pattern is also shown in the inset. (b) RSMs of the 013 diffraction spot for the $(Ca,Sr,Ba)(Ti_{0.8}Nb_{0.2})O_3$ films. Dotted line, which corresponds to cubic lattice ($q_z/q_x=-3$), is also shown.

[a)]To whom correspondence should be addressed; electronic mail: koumoto@apchem.nagoya-u.ac.jp

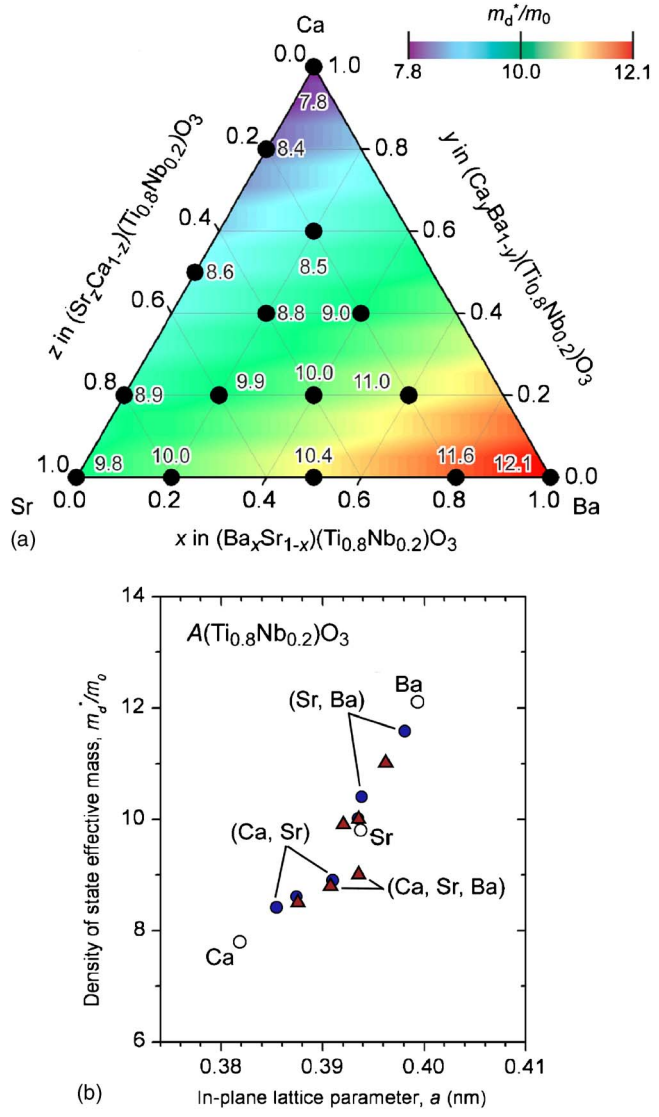

FIG. 2. (Color online) Density of states effective mass (m_d^*) of the $(Ca,Sr,Ba)(Ti_{0.8}Nb_{0.2})O_3$ films. (a) Compositional mapping of the m_d^*. The m_d^* values of the $Ca(Ti_{0.8}Nb_{0.2})O_3$, $Sr(Ti_{0.8}Nb_{0.2})O_3$, and $Ba(Ti_{0.8}Nb_{0.2})O_3$ films are $7.8m_0$, $9.8m_0$, and $12.1m_0$, respectively. (b) Plots for the m_d^* values vs in-plane lattice parameter (a).

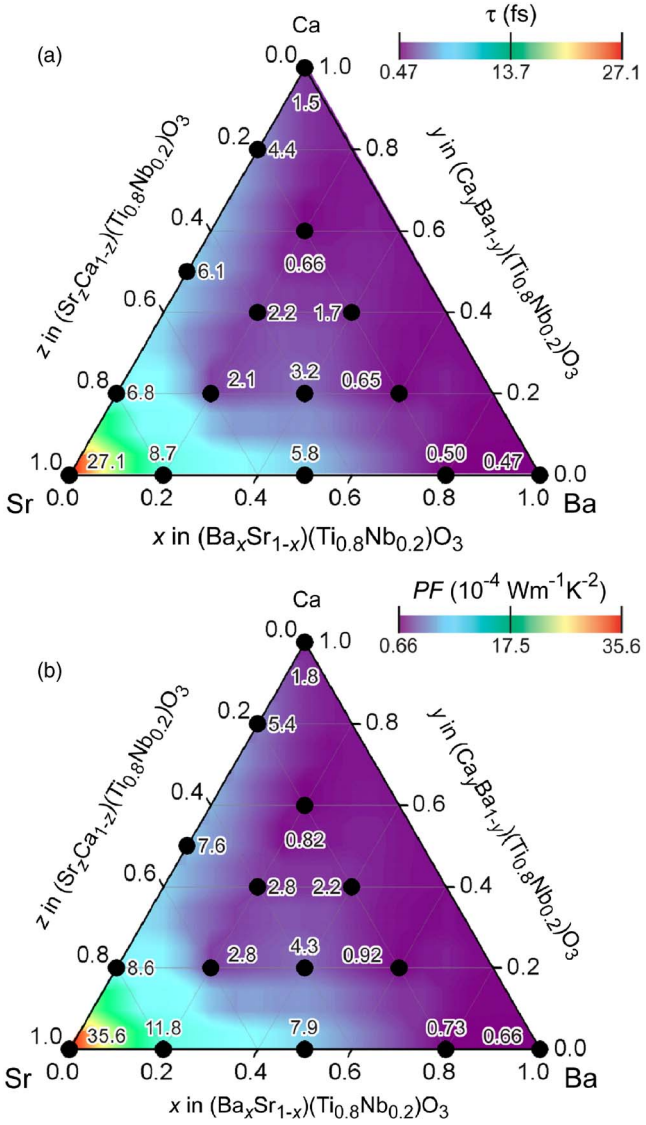

FIG. 3. (Color online) Compositional mapping of (a) Carrier relaxation time (τ) and (b) thermoelectric power factor ($PF=S^2\sigma$) for $(Ca,Sr,Ba)\times(Ti_{0.8}Nb_{0.2})O_3$ films at room temperature.

steps, which correspond to the unit cell height (~0.4 nm) of $(Ca,Sr,Ba)(Ti_{0.8}Nb_{0.2})O_3$, are clearly seen in the topographic AFM image of a $(Ca_{0.4}Sr_{0.2}Ba_{0.4})(Ti_{0.8}Nb_{0.2})O_3$ film [Fig. 1(a)]. From these results, we conclude that the film quality is sufficient to evaluate thermoelectric properties.

Figure 1(b) shows the x-ray reciprocal space mappings (RSMs) for the 013 diffraction spot of $(Ca,Sr,Ba)\times(Ti_{0.8}Nb_{0.2})O_3$ films. The dotted line, which corresponds to the cubic lattice ($q_z/q_x=-3$), is also shown. The 013 diffraction spot of $Sr(Ti_{0.8}Nb_{0.2})O_3$ film is located on the dotted line, indicating that the crystallographic symmetry of the film is cubic. However, those of $(Ca,Sr,Ba)(Ti_{0.8}Nb_{0.2})O_3$ and $(Sr,Ba)(Ti_{0.8}Nb_{0.2})O_3$ films slightly deviate from the dotted line, indicating that Sr-site substitution in $Sr(Ti_{0.8}Nb_{0.2})O_3$ with Ca and/or Ba induces an asymmetrical lattice expansion.

The carrier concentration (n_e) and Hall mobility (μ_{Hall}) of the $(Ca,Sr,Ba)(Ti_{0.8}Nb_{0.2})O_3$ films were measured by the dc four probe method with a van der Pauw configuration at room temperature.[15] The Seebeck coefficient (S) was measured at room temperature by the conventional steady state method and by introducing a temperature gradient in the in-plane direction. The m_d^* value was calculated according to the following equations using the observed n_e and S values:

$$m_d^* = \frac{h^2}{2k_BT}\left[\frac{n_e}{4\pi F_{1/2}(\xi)}\right]^{2/3}, \tag{1}$$

$$F_r(\xi) = \int_0^\infty \frac{x^r}{1+e^{x-\xi}}dx, \tag{2}$$

$$S = -\frac{k_B}{e}\left[\frac{(r+2)F_{r+1}(\xi)}{(r+1)F_r(\xi)} - \xi\right], \tag{3}$$

where h, k_B, T (300 K), F_r, ξ, and r are Planck constant, the Boltzmann constant, absolute temperature, Fermi integral, chemical potential, and scattering parameter of relaxation time [0.5 (Ref. 9 and 10)], respectively. Figure 2(a) shows the composition mapping of the m_d^* values for the $(Ca,Sr,Ba)(Ti_{0.8}Nb_{0.2})O_3$ films.[16] The m_d^* values of the $Ca(Ti_{0.8}Nb_{0.2})O_3$, $Sr(Ti_{0.8}Nb_{0.2})O_3$, and $Ba(Ti_{0.8}Nb_{0.2})O_3$

TABLE I. Carrier concentration (n_e), Hall mobility (μ_{Hall}), and Seebeck coefficient (S) for the $(Ca,Sr,Ba)(Ti_{0.8}Nb_{0.2})O_3$ epitaxial films at room temperature.

A-site comp. of $A(Ti_{0.8}Nb_{0.2})O_3$	n_e (10^{21} cm^{-3})	μ_{Hall} (cm^2 V^{-1} s^{-1})	S (μV K^{-1})
Ca	1.5	0.33	−147
$Ca_{0.8}Sr_{0.2}$	3.2	0.92	−106
$Ca_{0.5}Sr_{0.5}$	2.5	1.3	−123
$Ca_{0.2}Sr_{0.8}$	3.3	1.3	−111
Sr	3.9	4.9	−108
$Sr_{0.8}Ba_{0.2}$	3.0	1.5	−128
$Sr_{0.5}Ba_{0.5}$	4.1	0.97	−111
$Sr_{0.2}Ba_{0.8}$	3.0	0.076	−142
Ba	7.2	0.068	−92
$Ca_{0.8}Sr_{0.2}Ba_{0.2}$	1.7	0.14	−148
$Ca_{0.2}Sr_{0.8}Ba_{0.2}$	3.1	0.37	−123
$Ca_{0.2}Sr_{0.2}Ba_{0.6}$	3.0	0.10	−136
$Ca_{0.4}Sr_{0.4}Ba_{0.2}$	2.6	0.44	−124
$Ca_{0.4}Sr_{0.2}Ba_{0.4}$	2.5	0.34	−129
$Ca_{0.2}Sr_{0.4}Ba_{0.4}$	4.0	0.56	−109

films are $7.8m_0$, $9.8m_0$, and $12.1m_0$, respectively. A nearly linear relationship is clearly seen in the plots of the m_d^* values as a function of the in-plane lattice parameter (a) [Fig. 2(b)]. This clearly indicates that lattice expansion leads to an enhanced m_d^* because the overlap population of Ti $3d$-t_{2g} orbitals decreases with the Ti–Ti distance.

We then calculated the τ value of the $(Ca,Sr,Ba)\times(Ti_{0.8}Nb_{0.2})O_3$ films according to the following equation:

$$\tau = \frac{\mu_{\mathrm{Hall}} m_d^*}{e}.$$

Figure 3(a) summarizes the calculated τ values for the $(Ca,Sr,Ba)(Ti_{0.8}Nb_{0.2})O_3$ films. The τ values of $Ca(Ti_{0.8}Nb_{0.2})O_3$, $Sr(Ti_{0.8}Nb_{0.2})O_3$, and $Ba(Ti_{0.8}Nb_{0.2})O_3$ films are 1.5, 27.1, and 0.47 fs, respectively. The τ value of $Sr(Ti_{0.8}Nb_{0.2})O_3$ drastically decreases when the Sr site is substituted with Ca and/or Ba. This decrease may be due to the asymmetrical expansion of the TiO_6 octahedra, which reduces the linearity of the electron conduction paths. A similar compositional phase diagram is obtained in the thermoelectric power factor ($PF=S^2\sigma$) for the $(Ca,Sr,Ba)\times(Ti_{0.8}Nb_{0.2})O_3$ films [Fig. 3(b)]. These results indicate that Ca and/or Ba substitution for Sr in $Sr(Ti_{0.8}Nb_{0.2})O_3$ negatively affects the thermoelectric performance of $Sr(Ti_{0.8}Nb_{0.2})O_3$ because these substitutions seriously reduce σ.

In summary, herein we have proposed a thermoelectric phase diagram for the $(Ca,Sr,Ba)(Ti_{0.8}Nb_{0.2})O_3$ system. Although the m_d^* value almost proportionally increases with the in-plane lattice parameter of $(Ca,Sr,Ba)(Ti_{0.8}Nb_{0.2})O_3$ film, the τ value drastically decreases when Sr is substituted by Ca and/or Ba in $Sr(Ti_{0.8}Nb_{0.2})O_3$, which implies that Sr-site substitution with Ca and/or Ba negatively affects the thermoelectric performance of $Sr(Ti_{0.8}Nb_{0.2})O_3$. The fact that the solid solution affects the carrier transport properties is useful for the design concept of thermoelectric materials.

This work was financially supported by the Industrial Technology Research Grant Program in 2005 from the New Energy and Industrial Technology Development Organization (NEDO) and Grant-in-Aid for Scientific Research from the Ministry of Education, Culture, Sports, Science and Technology (No. 18686054).

[1] H. P. R. Frederikse, W. R. Thurber, and W. R. Hosler, Phys. Rev. **134**, A442 (1964).
[2] T. Caillat, A. Borshchevsky, and J. P. Fleurial, J. Appl. Phys. **80**, 4442 (1996).
[3] T. Okuda, K. Nakanishi, S. Miyasaka, and Y. Tokura, Phys. Rev. B **63**, 113104 (2001).
[4] I. Terasaki, Y. Sasago, and K. Uchinokura, Phys. Rev. B **56**, R12685 (1997).
[5] Y. Wang, N. S. Rogado, R. J. Cava, and N. P. Ong, Nature (London) **423**, 425 (2003).
[6] R. Funahashi, I. Matsubara, H. Ikuta, T. Takeuchi, U. Mizutani, and S. Sodeoka, Jpn. J. Appl. Phys., Part 2 **39**, L1127 (2000).
[7] M. Shikano and R. Funahashi, Appl. Phys. Lett. **82**, 1851 (2003).
[8] K. Sugiura, H. Ohta, K. Nomura, M. Hirano, H. Hosono, and K. Koumoto, Appl. Phys. Lett. **89**, 032111 (2006).
[9] S. Ohta, T. Nomura, H. Ohta, M. Hirano, H. Hosono, and K. Koumoto, Appl. Phys. Lett. **87**, 092108 (2005).
[10] S. Ohta, T. Nomura, H. Ohta, and K. Koumoto, J. Appl. Phys. **97**, 034106 (2005).
[11] S. Ohta, H. Ohta, and K. Koumoto, J. Ceram. Soc. Jpn. **97**, 034106 (2005).
[12] H. Muta, A. Ieda, K. Kurosaki, and S. Yamanaka, Mater. Lett. **58**, 3868 (2004).
[13] H. Muta, K. Kurosaki, and S. Yamanaka, J. Alloys Compd. **368**, 22 (2004).
[14] T. Ohnishi, K. Takahashi, M. Nakamura, M. Kawasaki, M. Yoshimoto, and H. Koinuma, Appl. Phys. Lett. **74**, 2531 (1999).
[15] The carrier concentration (n_e), Hall mobility (μ_{Hall}), and Seebeck coefficient (S) for the $(Ca,Sr,Ba)(Ti_{0.8}Nb_{0.2})O_3$ epitaxial films at room temperature are summarized in Table I.
[16] A single-phase film of $(Ca,Ba)(Ti_{0.8}Nb_{0.2})O_3$ was not obtained possibly because the size difference between Ca^{2+} (134 pm) and Ba^{2+} (161 pm) suppresses the formation of a homogeneous solid solution.